

## Temperature-pressure phase diagram and ferroelectric properties of BaTiO<sub>3</sub> single crystal based on a modified Landau potential

J. J. Wang, P. P. Wu, X. Q. Ma, and L. Q. Chen

Citation: *J. Appl. Phys.* **108**, 114105 (2010); doi: 10.1063/1.3504194

View online: <http://dx.doi.org/10.1063/1.3504194>

View Table of Contents: <http://jap.aip.org/resource/1/JAPIAU/v108/i11>

Published by the [American Institute of Physics](#).

---

### Related Articles

Misfit strain dependence of ferroelectric and piezoelectric properties of clamped (001) epitaxial Pb(Zr<sub>0.52</sub>Ti<sub>0.48</sub>)O<sub>3</sub> thin films  
*Appl. Phys. Lett.* **99**, 252904 (2011)

Phase transitions in ferroelectric-paraelectric superlattices  
*J. Appl. Phys.* **110**, 114109 (2011)

Dielectric and nonlinear current–voltage characteristics of rare–earth doped CaCu<sub>3</sub>Ti<sub>4</sub>O<sub>12</sub> ceramics  
*J. Appl. Phys.* **110**, 094101 (2011)

Scanning electro-optic microscopy of ferroelectric domain structure with a near-field fiber probe  
*J. Appl. Phys.* **110**, 084117 (2011)

Ferroelectric domains in epitaxial PbTiO<sub>3</sub> films on LaAlO<sub>3</sub> substrate investigated by piezoresponse force microscopy and far-infrared reflectance  
*J. Appl. Phys.* **110**, 084115 (2011)

---

### Additional information on *J. Appl. Phys.*

Journal Homepage: <http://jap.aip.org/>

Journal Information: [http://jap.aip.org/about/about\\_the\\_journal](http://jap.aip.org/about/about_the_journal)

Top downloads: [http://jap.aip.org/features/most\\_downloaded](http://jap.aip.org/features/most_downloaded)

Information for Authors: <http://jap.aip.org/authors>

### ADVERTISEMENT

**AIP**Advances

*Submit Now*

**Explore AIP's new  
open-access journal**

- **Article-level metrics  
now available**
- **Join the conversation!  
Rate & comment on articles**

# Temperature-pressure phase diagram and ferroelectric properties of BaTiO<sub>3</sub> single crystal based on a modified Landau potential

J. J. Wang,<sup>1,2</sup> P. P. Wu,<sup>1,2</sup> X. Q. Ma,<sup>2,a)</sup> and L. Q. Chen<sup>1</sup>

<sup>1</sup>*Department of Materials Science and Engineering, Pennsylvania State University, University Park, Pennsylvania 16802, USA*

<sup>2</sup>*Department of Physics, University of Science and Technology Beijing, Beijing 100083, China*

(Received 1 July 2010; accepted 18 September 2010; published online 6 December 2010)

A modified eighth-order Landau potential was proposed for the BaTiO<sub>3</sub> single crystal by taking account into the quantum mechanical effects at low temperature. While all existing thermodynamic potentials for BaTiO<sub>3</sub> fail to accurately describe the pressure dependence of ferroelectric transition temperatures, the temperature and hydrostatic pressure phase diagram constructed using the modified potential shows excellent agreement with experimental measurements by Ishidate, Abe, Takahashi, and Mori [Phys. Rev. Lett. **78**, 2397 (1997)]. On the basis of the new proposed Landau potential, we calculated the dielectric coefficients, spontaneous polarizations, temperature-electric field phase diagram, and piezoelectric coefficients, all in good agreement well with existing experimental data. © 2010 American Institute of Physics. [doi:10.1063/1.3504194]

## I. INTRODUCTION

As a classic ferroelectric, the thermodynamics of BaTiO<sub>3</sub> is the most extensively studied over half a century<sup>1–7</sup> since Devonshire wrote down a sixth-order classic Landau potential to describe the thermodynamics of phase transitions in BaTiO<sub>3</sub>.<sup>1</sup> Bell and Cross reported a set of sixth-order Landau polynomial potential coefficients by assuming three of them temperature-dependent. Li, *et al.*,<sup>7</sup> proposed an eighth-order Landau potential for predicting the phase transitions, domain structures, and other properties of BaTiO<sub>3</sub> for both thin films and bulk crystals.<sup>7–11</sup> Finally, Wang, *et al.*,<sup>12</sup> proposed another eighth-order Landau potential by arguing that the second and higher-order coefficients should be temperature-dependent to describe adequately the thermodynamic behavior of BaTiO<sub>3</sub>. The classical Landau potentials have been reasonably successful in describing the phase transitions and ferroelectric properties of BaTiO<sub>3</sub> above the so-called saturation temperature above which the quantum mechanical effects can be neglected.<sup>13</sup>

The phase transitions and properties of a ferroelectric can be modified by external fields such as biaxial or uniaxial stress, hydrostatic pressure, or electric field. The focus of this work is on the pressure dependence of transition temperature, represented by the pressure-temperature phase diagram. Both first principle studies and experimental measurement showed that the phase transitions of bulk BaTiO<sub>3</sub> from paraelectric phase to ferroelectric phase and from the parallel phase to ferroelectric phase should be first-order,<sup>14–17</sup> thus the phase boundaries can be discussed using the Clapeyron equation. On a pressure-temperature phase diagram, the pressure dependence of a transition temperature is described by the Clapeyron relation,  $dp/dT=L/T\Delta V=\Delta S/\Delta V$ , where  $dp/dT$  is the slope of the two-phase coexistence curve,  $L$  the latent heat,  $\Delta S$  the entropy change,  $T$  the transition temperature,  $\Delta V$  the volume change. In the classical limit,  $\Delta S$  is approximately proportional to  $\Delta V$ , hence the pressure depen-

dence of transition temperature is also approximately linear.<sup>18,19</sup> However, at low temperature near 0 K, the quantum theory predicts:  $T_C(p) \propto (p_C - p)^{1/2}$ , where  $T_C$  is the transition temperature,  $p$  is the hydrostatic pressure and  $p_C$  is its value at  $T_C=0$  K.<sup>19–21</sup> Therefore, in order to accurately describe the dependence of the transition temperatures on external fields including those below the saturation temperature, the effect of quantum fluctuation such as zero-point vibration on vibrational mode of the lattice should be considered.

The dielectric constants, polarizations, and phase transitions under hydrostatic pressure were experimentally studied by Samara *et al.* in 1966,<sup>22</sup> Decker and Zhao in 1989,<sup>23</sup> and Ishidate *et al.* in 1997.<sup>24</sup> Samara *et al.* considered hydrostatic pressures up to 2.5 GPa. It was shown that the transition temperature decreases with hydrostatic pressure and a triple point was obtained by classical extrapolation.<sup>22</sup> A similar measurement was performed by Decker *et al.* for hydrostatic pressure up to 3.8 GPa. They showed that the cubic to tetragonal ferroelectric phase transition in BaTiO<sub>3</sub> under hydrostatic pressure was displacive and became less discontinuous as pressure was increased until a triple point was reached at about 3.5 GPa and  $-40$  °C. Furthermore, it was demonstrated that the peak values for the dielectric constants increased with hydrostatic pressure. A more recent and thorough measurement was conducted by Ishidate *et al.* determined the BaTiO<sub>3</sub> temperature-pressure phase diagram for pressures up to 10 GPa and temperatures down to 4 K, resulting in a relatively complete pressure-temperature phase diagram including both the classical limit above the saturation temperature and the quantum limit below the saturation temperature. They also obtained three critical pressures of 5.4, 6.0, and 6.5 GPa at which the rhombohedral, orthorhombic, or tetragonal phase disappears, respectively, over the whole temperature range. The pressure-temperature phase diagram obtained by Zhong *et al.*<sup>15</sup> using first principle calculations, although there are quantitative differences, qualitatively agrees with Ishidate's experimentally measured phase diagram. Jorge *et al.* recalculated the pressure-temperature phase diagram of

<sup>a)</sup>Electronic mail: xqma@sas.ustb.edu.cn.

BaTiO<sub>3</sub> by considering the zero-point motion of ions and using theoretically perfect hydrostatic pressure. The recalculated phase diagram by first principles corroborated Ishide's experimental results.<sup>25</sup>

To correctly describe the phase transitions at low temperatures using a phenomenological description, Salje *et al.* included the quantum mechanical effects in the classical Landau potential.<sup>4-6,13,18</sup> For example, Salje *et al.* employed a modified Landau-type expression for the Gibbs energy by including the saturation effects of order parameter to describe the variation in the order parameter with temperature for As<sub>2</sub>O<sub>5</sub>, LaAlO<sub>3</sub>, CaCO<sub>3</sub>, NaNO<sub>3</sub>, Pb<sub>3</sub>(PO<sub>4</sub>)<sub>2</sub>, etc.<sup>13</sup> and the obtained results were in excellent agreement with experimental measurements. Salje *et al.* also computed the temperature-pressure or temperature-composition phase diagrams for SrTiO<sub>3</sub>, KH<sub>2</sub>PO<sub>4</sub>, KTaO<sub>3</sub>, and SbSI using Landau theory with quantum effects.<sup>18</sup> Hayward *et al.* determined the pressure-temperature phase diagram of BaTiO<sub>3</sub> based on the Landau description proposed by Salje *et al.*<sup>6</sup> However, due to the complexity of multiple phase transitions in BaTiO<sub>3</sub>, their model was not able to predict the orthorhombic to rhombohedral phase transition. There has also been no systematic theoretical study on the physical properties of BaTiO<sub>3</sub> under a hydrostatic pressure.<sup>6</sup> Therefore, the main objective of this work is to analyze the effect of hydrostatic pressure on ferroelectric phase transitions as well as ferroelectric properties in BaTiO<sub>3</sub>. For this purpose, we modified the eighth-order thermodynamic potential for BaTiO<sub>3</sub> by connecting the classical and quantum limits following the work of Salje *et al.*<sup>7</sup>

The paper is organized as follows. In Sec. II, we describe the modified Landau potential and the determination of the coefficients. In Sec. III, a temperature-pressure phase diagram is constructed based on the new Landau potential coefficients. We compared the predicted results with those obtained by experiments as well as with those obtained using the classical Landau potential without including the quantum effects. In Sec. IV, the dielectric constants under a hydrostatic pressure are calculated and are compared with existing experimental data. In Sec. V, the phase transitions under an electric field along [001], [101], and [111] directions are studied. In Sec. VI, the electric field induced strains and piezoelectric coefficients are discussed. Finally, we summarize the results in Sec. VII.

## II. LANDAU THERMODYNAMIC POTENTIAL

Taking the cubic paraelectric phase as the reference, the Gibbs free energy as a function of polarization under stress can be expressed as

$$\begin{aligned} \Delta G = & f_{\text{LGD}} - \frac{1}{2}s_{11}(\sigma_1^2 + \sigma_2^2 + \sigma_3^2) - s_{12}(\sigma_1\sigma_2 + \sigma_1\sigma_3 \\ & + \sigma_2\sigma_3) - \frac{1}{2}s_{44}(\sigma_4^2 + \sigma_5^2 + \sigma_6^2) - Q_{11}(\sigma_1P_1^2 + \sigma_2P_2^2 \\ & + \sigma_3P_3^2) - Q_{12}[\sigma_1(P_2^2 + P_3^2) + \sigma_2(P_1^2 + P_3^2) + \sigma_3(P_2^2 \\ & + P_1^2)] - Q_{44}(\sigma_4P_2P_3 + \sigma_5P_1P_3 + \sigma_6P_2P_1), \end{aligned} \quad (1)$$

with

$$\begin{aligned} f_{\text{LGD}} = & \alpha_1(P_1^2 + P_2^2 + P_3^2) + \alpha_{11}(P_1^4 + P_2^4 + P_3^4) + \alpha_{12}(P_1^2P_2^2 \\ & + P_1^2P_3^2 + P_2^2P_3^2) + \alpha_{123}P_1^2P_2^2P_3^2 + \alpha_{111}(P_1^6 + P_2^6 \\ & + P_3^6) + \alpha_{112}[P_1^2(P_2^4 + P_3^4) + P_2^2(P_1^4 + P_3^4) + P_3^2(P_1^4 \\ & + P_2^4)] + \alpha_{1111}(P_1^8 + P_2^8 + P_3^8) + \alpha_{1122}(P_1^4P_2^4 + P_1^4P_3^4 \\ & + P_2^4P_3^4) + \alpha_{1112}[P_1^6(P_2^2 + P_3^2) + P_2^6(P_1^2 + P_3^2) \\ & + P_3^6(P_1^2 + P_2^2)] + \alpha_{1123}(P_1^4P_2^2P_3^2 + P_1^2P_2^4P_3^2 \\ & + P_1^2P_2^2P_3^4), \end{aligned} \quad (2)$$

where  $P_i$  is the  $i$ th component of polarization,  $\sigma_i$   $i$ th component of applied stress in Voigt notation,  $s_{11}$ ,  $s_{12}$ , and  $s_{44}$  the elastic compliance constants of cubic phase, and  $Q_{11}$ ,  $Q_{12}$ , and  $Q_{44}$  the corresponding electrostrictive coefficients.

All the Landau potential coefficients in Eq. (2) are assumed to be temperature-independent except  $\alpha_1$ . The  $T_S$  included in  $\alpha_1$  is named the saturation temperature below which the quantum mechanical effects are significant. We use the same saturation temperature (160 K) as in Salje *et al.*'s work.<sup>6</sup> The main difference from the existing eighth-order Landau potential<sup>7</sup> is the fact that  $\alpha_{11}$ ,  $\alpha_{12}$ ,  $\alpha_{111}$ ,  $\alpha_{112}$ , and  $\alpha_{123}$  in the modified potential are dependent on the applied stress (see Table I for the specific dependencies). The stress dependences of  $\alpha_{11}$ ,  $\alpha_{12}$ ,  $\alpha_{111}$ ,  $\alpha_{112}$ , and  $\alpha_{123}$  represent the higher-order electrostrictive coupling between stress and polarization. Such high-order electrostrictive coupling was discussed as early as in the 1950s on the electric field induced strains  $\varepsilon = bE^2 + dE^4 + fE^6 + \dots$ .<sup>26</sup> Although the first term is sufficient for most purposes, the higher-order anharmonic terms are necessary in order to account for the thermal expansion. In the case of cubic BaTiO<sub>3</sub>, for instance, the departure of the oxygen potential wells from being truly harmonic is one of the important features of the theory, explained by Devonshire and Slater.<sup>1,27</sup> Furthermore, the presence of higher-order terms is also used to explain the experimentally observed temperature dependence of the dielectric susceptibility.<sup>26</sup> Similarly, one can also write the general polarization dependence of strain through,  $\varepsilon = bP^2 + dP^4 + fP^6 + \dots$ . Under high hydrostatic pressure, the higher-order coupling between stress and polarization is required to account for the accurate pressure-temperature phase diagram.

The coefficients obtained in this work along with those from a number of previous works are shown in Table I. It should be noted that the existing thermodynamic potentials were obtained by fitting the coefficients to the properties of BaTiO<sub>3</sub> under zero pressure. Therefore, the existing coefficients may not be applicable for describing properties under hydrostatic pressure. In this work,  $\alpha_{11}$ ,  $\alpha_{111}$ , and  $\alpha_{1111}$  were obtained using the properties of the tetragonal phase under pressure, including the cubic to tetragonal transition temperature, and the spontaneous polarization and the dielectric constants of the tetragonal phase. Similarly,  $\alpha_{12}$ ,  $\alpha_{112}$ ,  $\alpha_{1122}$ , and  $\alpha_{1112}$  were fitted to the properties of the orthorhombic phase, and  $\alpha_{123}$  and  $\alpha_{1123}$  to the properties of the rhombohedral phase. While  $\alpha_1$  is assumed to be linearly dependent on temperature in the classical approximation,<sup>1,3,7</sup>  $\alpha_1$  is assumed to be a hyperbolic cotangent function of temperature to include quantum effects as it was proposed by Salje *et al.*<sup>6,13,18</sup>

TABLE I. Coefficients of Landau potential in Eq. (2), where  $T$  is temperature in kelvin,  $T_S$  is the saturation temperature below which the quantum mechanical effects are not ignorable, and  $\sigma_1$ ,  $\sigma_2$ , and  $\sigma_3$  are stress along x, y, and z direction in unit of gigapascal.

Coefficients	This Work	Bell and Cross	Li <i>et al.</i>	Wang <i>et al.</i>	Units
$\alpha_1$	$5.0 \times 10^5 \times T_S$ $\times \left[ \text{Coth}\left(\frac{T_S}{T}\right) - \text{Coth}\left(\frac{T_S}{390}\right) \right]$	$3.34 \times 10^5$ $\times (T-381)$	$4.124 \times 10^5$ $\times (T-388)$	$3.61 \times 10^5$ $\times (T-391)$	$\text{V m C}^{-1}$
$\alpha_{11}$	$-1.154 \times 10^8$ $\times [1+0.037(\sigma_1+\sigma_2+\sigma_3)]$	$4.69 \times 10^6 \times (T-393)$ $-2.02 \times 10^8$	$-2.097 \times 10^8$	$-1.83 \times 10^9$ $+4.0 \times 106T$	$\text{V m}^5 \text{C}^{-3}$
$\alpha_{12}$	$6.530 \times 10^8$ $\times [1+0.037(\sigma_1+\sigma_2+\sigma_3)]$	$3.230 \times 10^8$ $-5.52 \times 107 \times (T-393)$	$7.974 \times 10^8$	$+6.7 \times 106T$ $1.39 \times 1010$	$\text{V m}^5 \text{C}^{-3}$
$\alpha_{111}$	$-2.106 \times 10^9$ $\times [1+0.023(\sigma_1+\sigma_2+\sigma_3)]$	$+2.76 \times 10^9$	$1.294 \times 10^9$	$-3.2 \times 107T$	$\text{V m}^9 \text{C}^{-5}$
$\alpha_{112}$	$4.091 \times 10^9$ $\times [1+0.023(\sigma_1+\sigma_2+\sigma_3)]$	$4.470 \times 10^9$	$-1.950 \times 10^9$	$-2.2 \times 10^9$	$\text{V m}^9 \text{C}^{-5}$
$\alpha_{123}$	$-6.688 \times 10^9$ $\times [1+0.023(\sigma_1+\sigma_2+\sigma_3)]$	$4.910 \times 10^9$	$-2.500 \times 10^9$	$5.51 \times 10^{10}$	$\text{V m}^9 \text{C}^{-5}$
$\alpha_{1111}$	$7.590 \times 10^{10}$	0.0	$3.863 \times 10^{10}$	$4.84 \times 10^{10}$	$\text{V m}^{13} \text{C}^{-7}$
$\alpha_{1112}$	$-2.193 \times 10^{10}$	0.0	$2.529 \times 10^{10}$	$2.53 \times 10^{11}$	$\text{V m}^{13} \text{C}^{-7}$
$\alpha_{1122}$	$-2.221 \times 10^{10}$	0.0	$1.637 \times 10^{10}$	$2.80 \times 10^{11}$	$\text{V m}^{13} \text{C}^{-7}$
$\alpha_{1123}$	$2.416 \times 10^{10}$	0.0	$1.367 \times 10^{10}$	$9.35 \times 10^{10}$	$\text{V m}^{13} \text{C}^{-7}$

Since only the second-order coefficient in the Landau free energy is temperature-dependent, the entropy change for a phase transition at the transition temperature can be obtained from  $\Delta S = [P_{\text{product}}^2(T_C) - P_{\text{parent}}^2(T_C)] / 2\varepsilon_0 C$ , where  $\varepsilon_0$  is the permittivity of vacuum and  $C$  is the Curie–Weiss constant.<sup>28</sup> Therefore, the entropy changes obtained in our work are  $13\,361 \text{ J m}^{-3} \text{ K}^{-1}$  for cubic to tetragonal phase transition,  $9237 \text{ J m}^{-3} \text{ K}^{-1}$  for tetragonal to orthorhombic, and  $5531 \text{ J m}^{-3} \text{ K}^{-1}$  for orthorhombic to rhombohedral. For comparison, the entropy changes in Li *et al.*'s work are  $13\,535 \text{ J m}^{-3} \text{ K}^{-1}$ ,  $6640 \text{ J m}^{-3} \text{ K}^{-1}$ , and  $6971 \text{ J m}^{-3} \text{ K}^{-1}$ , respectively.<sup>7</sup> These values are in general agreement with experimental values listed in Ref. 28:  $13\,098$ – $13\,644$ ,  $5898$ – $9940$ , and  $4357$ – $7624 \text{ J m}^{-3} \text{ K}^{-1}$ .

### III. TEMPERATURE-PRESSURE PHASE DIAGRAM

Under a hydrostatic pressure, the applied stress tensors satisfy  $\sigma_1 = \sigma_2 = \sigma_3 = -p$ ,  $\sigma_4 = \sigma_5 = \sigma_6 = 0$ , and Eq. (1) becomes

$$\Delta G = f_{\text{LGD}} - \left( \frac{3}{2}s_{11} + 3s_{12} \right) p^2 + p(Q_{11} + 2Q_{12}) \times (P_1^2 + P_2^2 + P_3^2). \quad (3)$$

The variation in polarization with temperature and pressure was obtained and shown in Figs. 1(a) and 1(b). Each phase transition can easily be identified in Fig. 1 based on the jumps in polarization values. Application of a hydrostatic pressure decreases polarization at a given temperature. As the hydrostatic pressure increases, the rhombohedral phase disappears first at its critical pressure, followed by the disappearance of the orthorhombic phase at 5.8 GPa, and finally, the tetragonal phase at about 6.4 GPa.

With the coefficients listed in Table I, a temperature-pressure phase diagram was constructed and shown in Fig. 2. We also included the experimental data from Ishidate's work<sup>24</sup> and theoretical results calculated by using classical Landau coefficients of Li *et al.* It can be seen from Fig. 2 that

the classical Landau potential coefficients of Li *et al.* produced linear dependence of transition temperatures on the hydrostatic pressure for all three phase transitions, rhombohedral to orthorhombic, orthorhombic to tetragonal, and tetragonal to cubic. While the transition temperatures obtained using the classical Landau potential coefficients of Li *et al.* show good agreements with experimentally measured values above the saturation temperature, their linear dependence on

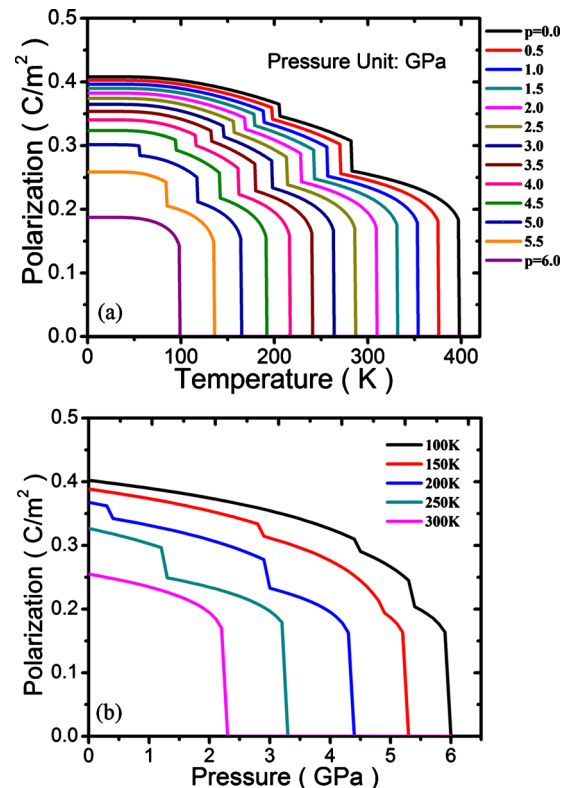


FIG. 1. (Color online) (a). Polarization of  $\text{BaTiO}_3$  vs temperature under different hydrostatic pressures. (b). Polarization of  $\text{BaTiO}_3$  vs hydrostatic pressure at different temperatures.

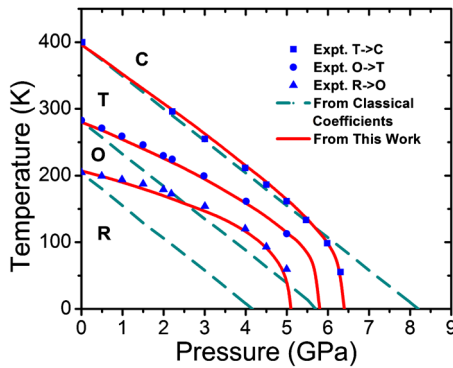


FIG. 2. (Color online) Temperature-pressure phase diagram of BaTiO<sub>3</sub>. The blue square, circle, and triangle indicate experimentally measured cubic-tetragonal phase boundary, tetragonal-orthorhombic phase boundary, and orthorhombic-rhombohedral phase boundary. The cyan solid line, dotted line, and dashed line indicate the cubic-tetragonal phase boundary, tetragonal-orthorhombic phase boundary, and orthorhombic-rhombohedral phase boundary calculated from classical Landau coefficients calculated. The red solid line, dotted line, and dashed line indicate phase boundaries obtained by this work.

pressure is inconsistent with experiments at low temperatures. On the other hand, the phase boundaries obtained by the new Landau coefficients agree well with experimental measurements over the entire temperature range. It should be pointed out that above the saturation temperature  $T_S$ , the slope of the phase boundary between the cubic and tetragonal phases is mainly decided by the electrostrictive coefficients ( $Q_{11}+2Q_{12}$ ). In this work, we used  $Q_{11}=0.11$ ,  $Q_{12}=-0.045$ , and  $Q_{44}=0.029$ .<sup>28,29</sup> However, the higher-order couplings between stress and polarization have a significant effect on the phase transitions at lower temperatures, i.e., on both the orthorhombic/tetragonal and rhombohedral/orthorhombic phase boundaries.

Using the new coefficients, the zero pressure transition temperatures from cubic to tetragonal, tetragonal to orthorhombic, and orthorhombic to rhombohedral phase are 396 K, 280 K, and 207 K, respectively, which are consistent with existing experimental data.<sup>30-34</sup> The critical pressures for tetragonal, orthorhombic, and rhombohedral phases are 5.1, 5.8, and 6.4, which also agree well with experimental values of 5.4 GPa, 6.0 GPa and 6.5 GPa, respectively.<sup>24</sup> The slopes for the cubic/tetragonal, tetragonal/orthorhombic, and orthorhombic/rhombohedral phase boundaries above the saturation temperature 160 K are  $-45$  K/GPa,  $-28$  K/GPa, and  $-18$  K/GPa, respectively.

The modified Landau potential was obtained according to the ferroelectric properties of bulk BaTiO<sub>3</sub> at zero stress. In order to study the phase transitions of BaTiO<sub>3</sub> thin films under equally biaxial or nonequally biaxial in-plane misfit strains,<sup>35-37</sup> One can use a Legendre transformation to transform the Gibbs-free energy as a function of stress into the Helmholtz free energy as a function of strain. The Helmholtz-free energy can be used to study the phase transitions of thin films and nanowires under strained boundary conditions. In this work, we focus on the properties of bulk BaTiO<sub>3</sub>, and the phase transitions for BaTiO<sub>3</sub> nanowires under different mechanical boundary conditions will be discussed in next paper.

#### IV. DIELECTRIC CONSTANTS UNDER PRESSURE

Dielectric constant is one of the most important properties for a ferroelectric, e.g., for capacitor applications. We calculated dielectric constants under hydrostatic pressure using the modified thermodynamic potential. We focused on the dielectric constants  $\epsilon_c$  along the polar directions, namely, the [001] direction for the tetragonal phase, the [011] direction for the orthorhombic phase, and the [111] direction for the rhombohedral phase. The relative dielectric stiffnesses  $\chi_{ij}$  are deduced from the second-order derivatives of the free energy function with respect to polarization,

$$\chi_{ij} = \epsilon_0 \frac{\partial^2 \Delta G}{\partial P_i \partial P_j}, \quad (4)$$

In the cubic phase,  $P_1=P_2=P_3=0$ ,

$$\chi_{11} = \chi_{22} = \chi_{33} = 2\epsilon_0(\alpha_1 + pQ_{11} + 2pQ_{12}), \quad (5)$$

$$\chi_{12} = \chi_{13} = \chi_{23} = 0. \quad (6)$$

In the tetragonal phase,  $P_1=P_2=0$ ,  $P_3 \neq 0$ ,

$$\chi_{11} = \chi_{22} = 2\epsilon_0(\alpha_1 + pQ_{11} + 2pQ_{12} + \alpha_{12}P_3^2 + \alpha_{112}P_3^4 + \alpha_{1112}P_3^6), \quad (7)$$

$$\chi_{33} = 2\epsilon_0(\alpha_1 + pQ_{11} + 2pQ_{12} + 6\alpha_{12}P_3^2 + 15\alpha_{111}P_3^4 + 28\alpha_{1111}P_3^6), \quad (8)$$

$$\chi_{12} = \chi_{13} = \chi_{23} = 0. \quad (9)$$

In the orthorhombic phase,  $P_1=0$ ,  $P_2=P_3 \neq 0$ ,

$$\chi_{11} = 2\epsilon_0(\alpha_1 + pQ_{11} + 2pQ_{12} + 2\alpha_{12}P_3^2 + 2\alpha_{112}P_3^4 + \alpha_{123}P_3^4 + 2\alpha_{1112}P_3^6 + 2\alpha_{1123}P_3^6), \quad (10)$$

$$\chi_{22} = \chi_{33} = 2\epsilon_0(\alpha_1 + pQ_{11} + 2pQ_{12} + 6\alpha_{11}P_3^2 + 15\alpha_{111}P_3^4 + 28\alpha_{1111}P_3^6 + \alpha_{12}P_3^2 + 7\alpha_{112}P_3^4 + 16\alpha_{1112}P_3^6 + 6\alpha_{1122}P_3^6), \quad (11)$$

$$\chi_{23} = 2\epsilon_0(2\alpha_{12}P_3^2 + 8\alpha_{112}P_3^4 + 12\alpha_{1112}P_3^6 + 8\alpha_{1122}P_3^6), \quad (12)$$

$$\chi_{12} = \chi_{13} = 0. \quad (13)$$

In the rhombohedral phase,  $P_1=P_2=P_3 \neq 0$ ,

$$\chi_{11} = \chi_{22} = \chi_{33} = 2\epsilon_0(\alpha_1 + pQ_{11} + 2pQ_{12} + 6\alpha_{11}P_3^2 + 15\alpha_{111}P_3^4 + 28\alpha_{1111}P_3^6 + \alpha_{12}P_3^2 + 14\alpha_{112}P_3^4 + \alpha_{123}P_3^4 + 32\alpha_{1112}P_3^6 + 12\alpha_{1122}P_3^6 + 8\alpha_{1123}P_3^6), \quad (14)$$

$$\chi_{12} = \chi_{13} = \chi_{23} = 2\epsilon_0(2\alpha_{12}P_3^2 + 8\alpha_{112}P_3^4 + 2\alpha_{123}P_3^4 + 12\alpha_{1112}P_3^6 + 8\alpha_{1122}P_3^6 + 10\alpha_{1123}P_3^6). \quad (15)$$

We make a coordinate transformation for each phase such that the polar direction is always along the [001] direction. The dielectric constant along the polar direction,  $\epsilon_c$ , and that

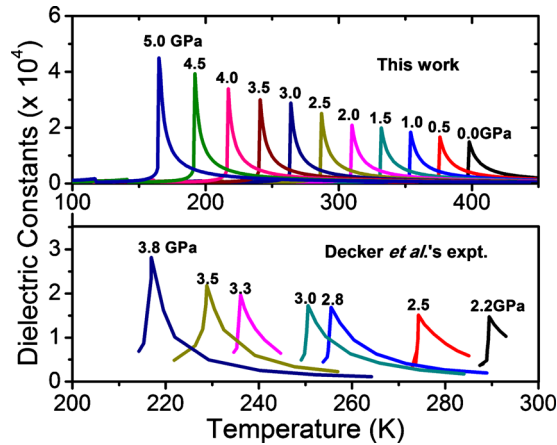


FIG. 3. (Color online) Dielectric constants  $\epsilon_c$  of BaTiO<sub>3</sub> single crystal versus temperature at different hydrostatic pressures, compared with Decker *et al.*'s experimental measurement result.

perpendicular to the polar direction,  $\epsilon_a$ , are given by

$$\text{In the cubic phase,} \quad \epsilon_a = \epsilon_c = \frac{1}{\chi_{33}}. \quad (16)$$

In the tetragonal phase,

$$\epsilon_a = \frac{1}{\chi_{11}}, \quad \epsilon_c = \frac{1}{\chi_{33}}. \quad (17)$$

In the orthorhombic phase,

$$\epsilon_a = \frac{1}{\chi_{11}}, \quad \epsilon_c = \frac{1}{\chi_{23} + \chi_{33}}. \quad (18)$$

In the rhombohedral phase,

$$\epsilon_a = \frac{1}{\chi_{11} - \chi_{12}}, \quad \epsilon_c = \frac{1}{\chi_{11} + 2\chi_{12}}. \quad (19)$$

Figure 3 shows the variation in dielectric constants  $\epsilon_c$  with temperature under different hydrostatic pressures. The results agree well with the experimental measurements of Decker and Zhao.<sup>23</sup> The dielectric constant displays peaks at each transition temperature. It is shown that the height of a peak increases with pressure, i.e., applied pressure enhances the dielectric response of a dielectric. It should be emphasized that the high-order electrostrictive couplings, i.e., the fourth- and sixth-order couplings between polarization and stress, are critical for the increase in the dielectric constant peaks with hydrostatic pressure.

Additional comparisons between theory and experimental on the temperature-dependent dielectric constants,  $\epsilon_a$  and  $\epsilon_c$  are plotted in Fig. 4.<sup>38</sup> It is shown that  $\epsilon_c$  values show much better agreement with experiments than those of  $\epsilon_a$  although our theoretical results for  $\epsilon_a$  qualitatively agrees with the experimental data. However, it is noted that there are significant differences among measured values for  $\epsilon_a$  from different sources. For example, in Merz's experiment,  $\epsilon_a:\epsilon_c$  is about 20:1 while in Mason and Matthias's experiment, the ratio is as high as 500:1.<sup>38,39</sup> Therefore, more accurate experimental measurements are needed for a more reliable comparison between theory and experiments for  $\epsilon_a$ .

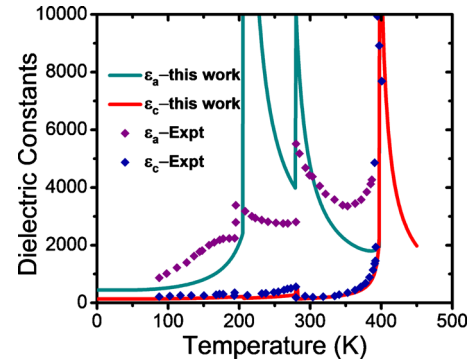


FIG. 4. (Color online) Dielectric constants  $\epsilon_a$  and  $\epsilon_c$  of BaTiO<sub>3</sub> single crystal vs temperature at zero hydrostatic pressures, compared with Merz's experimental measurement from 90 to 400 K.  $\epsilon_c$  is the dielectric constant along the polar direction, which is along [001] direction in tetragonal phase, [011] direction in orthorhombic phase, and [111] direction in rhombohedral phase. In our work  $\epsilon_a$  is along [100] direction in tetragonal and orthorhombic phase, along [110] in rhombohedral phase.

## V. TEMPERATURE-ELECTRIC FIELD PHASE DIAGRAM UNDER PRESSURE

The phase transitions in BaTiO<sub>3</sub> under an electric field in the stress-free condition were investigated by several groups for domain engineering and for understanding the role of electric field in phase transition of ferroelectrics.<sup>7,40-44</sup> With the presence of an applied external electric field, the Gibbs-free energy is rewritten as

$$\begin{aligned} \Delta G = & f_{\text{LGD}} - \frac{1}{2}s_{11}(\sigma_1^2 + \sigma_2^2 + \sigma_3^2) - s_{12}(\sigma_1\sigma_2 + \sigma_1\sigma_3 \\ & + \sigma_2\sigma_3) - \frac{1}{2}s_{44}(\sigma_4^2 + \sigma_5^2 + \sigma_6^2) - Q_{11}(\sigma_1P_1^2 + \sigma_2P_2^2 \\ & + \sigma_3P_3^2) - Q_{12}[\sigma_1(P_2^2 + P_3^2) + \sigma_2(P_1^2 + P_3^2) + \sigma_3(P_2^2 \\ & + P_1^2)] - Q_{44}(\sigma_4P_2P_3 + \sigma_5P_1P_3 + \sigma_6P_2P_1) - (E_1P_1 \\ & + E_2P_2 + E_3P_3). \end{aligned} \quad (20)$$

Here, we consider electric fields along [001], [101], and [111] directions. Based on Eq. (20), the temperature versus electric field phase diagrams are constructed. These phase diagrams are shown in Fig. 5 in (a), (b), and (c) for the electric field along [001], [010], or [111] direction, respectively. Because of the lack of experimental data, only phase transition under an electric field along the [001] direction is considered for comparison with experiment. With an applied field along [001] direction, BaTiO<sub>3</sub> undergoes a phase transition from the tetragonal phase to the first type of monoclinic phase labeled as M<sub>1</sub>, and then another from the M<sub>1</sub> phase to the distorted rhombohedral phase M<sub>2</sub>.<sup>45</sup> It can be seen that the phase boundaries calculated in this work agree well with Fesenko *et al.*'s experiment measurement.

## VI. STRAINS AND PIEZOELECTRIC COEFFICIENTS UNDER ELECTRIC FIELD

The strains under hydrostatic pressure can be derived from Eq. (20) by using the first-order derivatives of the Gibbs-free energy with respect to stress,

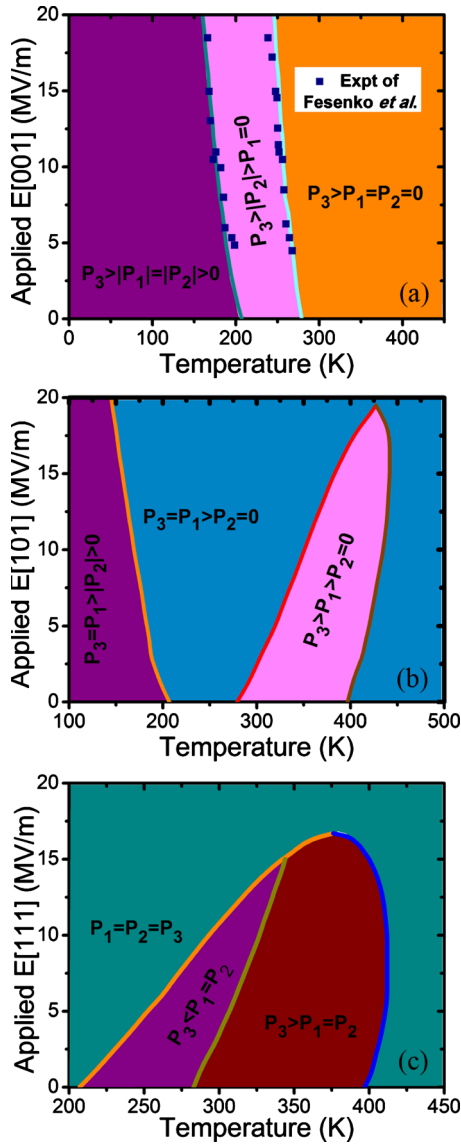


FIG. 5. (Color online) Phase transitions of BaTiO<sub>3</sub> single crystal under electric field along [001], [101], and [111] directions at stress-free condition. (a) Temperature-E[001] phase diagram, the squares of navy color indicate experimental data. (b) Temperature-E[101] phase diagram. (c) Temperature-E[111] phase diagram.

$$e_1 = - \left. \frac{\partial f_{\text{LGD}}}{\partial \sigma_1} \right|_{\sigma_1 = \sigma_2 = \sigma_3 = -p} + Q_{11}P_1^2 + Q_{12}(P_2^2 + P_3^2) - s_{11}p - 2s_{12}p, \quad (21)$$

$$e_2 = - \left. \frac{\partial f_{\text{LGD}}}{\partial \sigma_1} \right|_{\sigma_1 = \sigma_2 = \sigma_3 = -p} + Q_{11}P_2^2 + Q_{12}(P_1^2 + P_3^2) - s_{11}p - 2s_{12}p, \quad (22)$$

$$e_3 = - \left. \frac{\partial f_{\text{LGD}}}{\partial \sigma_1} \right|_{\sigma_1 = \sigma_2 = \sigma_3 = -p} + Q_{11}P_3^2 + Q_{12}(P_2^2 + P_1^2) - s_{11}p - 2s_{12}p, \quad (23)$$

$$e_4 = Q_{44}P_2P_3, \quad (24)$$

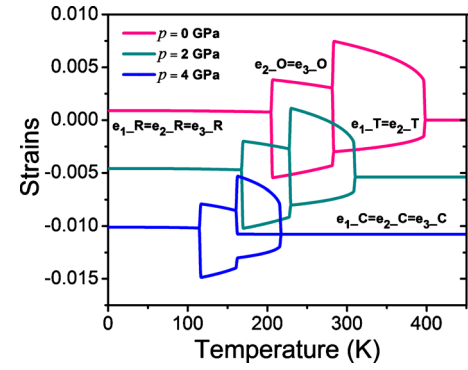


FIG. 6. (Color online) Elastic strains of BaTiO<sub>3</sub> single crystal under hydrostatic pressure of 0.0, 2.0, and 4.0 GPa. Counting from the right of the curves, the first stage is cubic phase where the strain components satisfy  $e_1 = e_2 = e_3$ , the second stage is tetragonal phase where the strain components satisfy  $e_1 = e_2 \neq e_3$ , the third stage is orthorhombic phase where the strain components satisfy  $e_1 \neq e_2 = e_3$  and the last stage is rhombohedral phase where the strain components satisfy  $e_1 = e_2 = e_3$ .

$$e_5 = Q_{44}P_1P_3, \quad (25)$$

$$e_6 = Q_{44}P_2P_1, \quad (26)$$

where only  $e_1$ ,  $e_2$ , and  $e_3$  are pressure-dependent. We employed the elastic compliance constants  $s_{11}$  and  $s_{12}$ ,  $9.07 \times 10^{-12}$  and  $-3.186 \times 10^{-12}$  m<sup>2</sup>/N, from Devonshire's work.<sup>1</sup>

Since some of the Landau potential coefficients are stress-dependent, the first term in  $e_1$ ,  $e_2$ , and  $e_3$  are the first derivative of Landau energy in Eq. (2) with respect to stress under a hydrostatic pressure condition. The strain variations with temperature under different hydrostatic pressures are shown in Fig. 6 where the normal strains  $e_1$ ,  $e_2$ , and  $e_3$  are plotted. The different colors in Fig. 6 indicate strain variations under different pressures, pink: zero hydrostatic pressure, dark: 2 GPa, and blue: 4 GPa. For each pressure, there are four stages, indicating the four phases of BaTiO<sub>3</sub>: cubic:  $e_1 = e_2 = e_3$ , tetragonal:  $e_1 = e_2 \neq e_3$ , orthorhombic:  $e_1 \neq e_2 = e_3$ , and rhombohedral phase:  $e_1 = e_2 = e_3$ . It can be seen from Fig. 6 that the strain curves are shifted to low left as hydrostatic pressure increases as a result of decrease in transition temperatures and strains under pressure.

A number of recent studies demonstrated that the piezoelectricity of BaTiO<sub>3</sub> could be enhanced by applying an electric field.<sup>41,42,46–48</sup> For example, Wada *et al.*'s experiment showed that with an electric field over 6 kV/cm along [111] direction, two continuous changes were observed in the strain-field curve, indicating the discontinuities in the piezoelectric coefficients under electric field along [111] direction.

Theoretically, the piezoelectric coefficients can be calculated from the first-order derivative of strains with respect to electric field. The strain  $e_{(lmn)}$  along any arbitrary direction with respect to the pseudocubic cell can be calculated through the following expression:

$$e_{(lmn)} = e_1l^2 + e_2m^2 + e_3n^2 + 2e_4mn + 2e_5ln + 2e_6lm, \quad (27)$$

where  $e_1$ ,  $e_2$ ,  $e_3$ ,  $e_4$ ,  $e_5$ , and  $e_6$  are obtained from Eqs. (21)–(26), and  $l, m, n$  are directional cosines that satisfy  $l^2 + m^2 + n^2 = 1$ .<sup>49</sup>

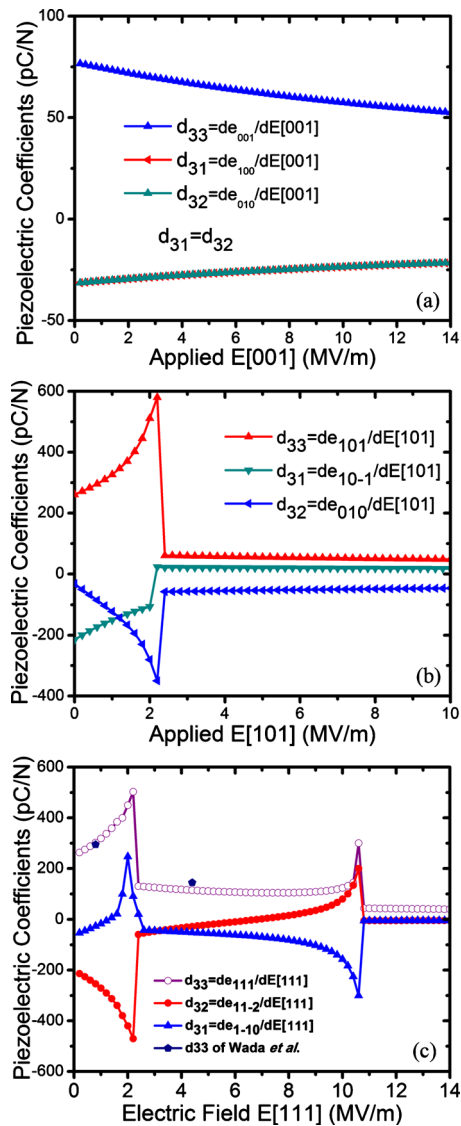


FIG. 7. (Color online) The piezoelectric coefficients  $d_{31}$ ,  $d_{32}$ , and  $d_{33}$  vs applied electric field at room temperature. (a) The electric field is along [001] direction. (b) The electric field is along [101] direction. (c) The electric field is along [111] direction, the pentagons with navy color indicate experimentally measured value of  $d_{33}$ .

We consider an electric field along [001], [101], or [111] directions. Piezoelectric coefficients were calculated along the field direction and other two orthogonal directions. Therefore, for the case of [001] direction, the three orthogonal directions are along [001], [010], and [100]; for [101] direction, they are [101],  $[10\bar{1}]$ , and [010]; for [111] direction, they are [111],  $[11\bar{2}]$ , and  $[1\bar{1}0]$ . Figure 7 shows the piezoelectric coefficients  $d_{31}$ ,  $d_{32}$ , and  $d_{33}$ . From Fig. 7 it can be seen that there are indeed two discontinuities for  $d_{33}$ ,  $d_{32}$ , and  $d_{31}$  with the electric field along [111] direction, and one discontinuity for  $d_{33}$ ,  $d_{32}$ , and  $d_{31}$  with the electric field along [101] direction, and all the discontinuities appear at the critical electric fields where a phase transition takes place. Our calculated  $d_{33}$  under zero pressure and room temperature agrees well with the measured value by Wada *et al.* indicated by two pentagons of navy blue color.<sup>41</sup> Finally, there is no discontinuity for piezoelectric coefficients at room tempera-

ture by applying electric field along the [001] direction, which is consistent with the fact that there is no ferroelectric phase transition in this case.

## VII. SUMMARY

A modified eighth-order Landau potential was proposed by introducing high-order electrocoupling effects and incorporating the quantum mechanical effects at low temperature for a single crystal BaTiO<sub>3</sub>. It leads to a temperature-pressure phase diagram that reproduces experimental results over the whole temperature range, overcoming the short-comings of all existing thermodynamic potentials for BaTiO<sub>3</sub>. The spontaneous polarization, dielectric constants, temperature-electric field phase diagram, and piezoelectric coefficients obtained using the new Landau coefficients all agree very well with existing experimental measurements.

## ACKNOWLEDGMENTS

This work was partially sponsored by the Project-Based Personnel Exchange Program by the China Scholarship Council and American Academic Exchange Service [(2008) 3012] National Science Foundation of China under Grant No. 50428101 and partially funded by NSF WMN Program under Grant No. DMR0908718 and NIRT Program under Grant No. DMR-0507146. The computations were performed using the Cyberstar cluster at the Pennsylvania State University, funded by the National Science Foundation through Grant No. OCI-0821527.

- <sup>1</sup>A. F. Devonshire, *Philos. Mag.* **40**, 1040 (1949).
- <sup>2</sup>P. W. Forsbergh, *Phys. Rev.* **93**, 686 (1954).
- <sup>3</sup>A. J. Bell and L. E. Cross, *Ferroelectrics* **59**, 197 (1984).
- <sup>4</sup>E. Salje, *Ferroelectrics* **104**, 111 (1990).
- <sup>5</sup>E. Salje and B. Wruck, *Ferroelectrics* **124**, 185 (1991).
- <sup>6</sup>S. A. Hayward and E. K. H. Salje, *J. Phys.: Condens. Matter* **14**, L599 (2002).
- <sup>7</sup>Y. L. Li, L. E. Cross, and L. Q. Chen, *J. Appl. Phys.* **98**, 064101 (2005).
- <sup>8</sup>Y. L. Li and L. Q. Chen, *Appl. Phys. Lett.* **88**, 072905 (2006).
- <sup>9</sup>V. Vaithyanathan, J. Lettieri, W. Tian, A. Sharan, A. Vasudevarao, Y. L. Li, A. Kochhar, H. Ma, J. Levy, P. Zschack, J. C. Woicik, L. Q. Chen, V. Gopalan, and D. G. Schlom, *J. Appl. Phys.* **100**, 024108 (2006).
- <sup>10</sup>Y. L. Li, S. Y. Hu, D. Tenne, A. Soukiasian, D. G. Schlom, X. X. Xi, K. J. Choi, C. B. Eom, A. Saxena, T. Lookman, Q. X. Jia, and L. Q. Chen, *Appl. Phys. Lett.* **91**, 252904 (2007).
- <sup>11</sup>G. Sheng, J. X. Zhang, Y. L. Li, S. Choudhury, Q. X. Jia, Z. K. Liu, and L. Q. Chen, *Appl. Phys. Lett.* **93**, 232904 (2008).
- <sup>12</sup>Y. L. Wang, A. K. Tagantsev, D. Damjanovic, N. Setter, V. K. Yarmarkin, A. I. Sokolov, and I. A. Lukyanchuk, *J. Appl. Phys.* **101**, 104115 (2007).
- <sup>13</sup>E. K. H. Salje, B. Wruck, and H. Thomas, *Z. Phys. B: Condens. Matter* **82**, 399 (1991).
- <sup>14</sup>W. Zhong, D. Vanderbilt, and K. M. Rabe, *Phys. Rev. Lett.* **73**, 1861 (1994).
- <sup>15</sup>W. Zhong, D. Vanderbilt, and K. M. Rabe, *Phys. Rev. B* **52**, 6301 (1995).
- <sup>16</sup>Landolt-Börnstein Numerical Data and Functional Relationships in Science and Technology, New Series, Group III, edited by E. Nakamura *et al.* (Springer-Verlag, Berlin, 1981), NS Group III, Vol. 16; edited by E. Nakamura *et al.*, NS Group III, Vol. 28.
- <sup>17</sup>M. H. Frey and D. A. Payne, *Phys. Rev. B* **54**, 3158 (1996).
- <sup>18</sup>S. A. Hayward and E. K. H. Salje, *J. Phys.: Condens. Matter* **10**, 1421 (1998).
- <sup>19</sup>T. Schneider, H. Beck, and E. Stoll, *Phys. Rev. B* **13**, 1123 (1976).
- <sup>20</sup>R. Morf, T. Schneider, and E. Stoll, *Phys. Rev. B* **16**, 462 (1977).
- <sup>21</sup>G. A. Samara, *Physica B & C* **150**, 179 (1988).
- <sup>22</sup>G. A. Samara, *Phys. Rev.* **151**, 378 (1966).
- <sup>23</sup>D. L. Decker and Y. X. Zhao, *Phys. Rev. B* **39**, 2432 (1989).
- <sup>24</sup>T. Ishidate, S. Abe, H. Takahashi, and N. Mori, *Phys. Rev. Lett.* **78**, 2397

- (1997).
- <sup>25</sup>J. Íñiguez and D. Vanderbilt, *Phys. Rev. Lett.* **89**, 115503 (2002).
- <sup>26</sup>H. F. Kay, *Rep. Prog. Phys.* **18**, 230 (1955).
- <sup>27</sup>J. C. Slater, *Phys. Rev.* **78**, 748 (1950).
- <sup>28</sup>F. Jona and G. Shirane, *Ferroelectric Crystals* (Macmillan, New York, 1962).
- <sup>29</sup>J. J. Wang, F. Y. Meng, X. Q. Ma, M. X. Xu, and L. Q. Chen, *J. Appl. Phys.* **108**, 034107 (2010).
- <sup>30</sup>J. F. Scott, *Ferroelectrics Memories* (Springer-Verlag, Berlin, 2000).
- <sup>31</sup>M. Lines and A. M. Glass, *Principles and Applications of Ferroelectrics and Related Materials* (Clarendon, Oxford, 1977).
- <sup>32</sup>F. Yona and G. Shirane, *Ferroelectric Crystals* (Pergamon, Oxford, 1962).
- <sup>33</sup>T. Mitsui, I. Tatsuzaki, and E. Nakamura, *An Introduction to the Physics of Ferroelectrics* (Maki-Shoten, Tokyo, 1976).
- <sup>34</sup>H. F. Kay and P. Vousden, *Philos. Mag.* **40**, 1019 (1949).
- <sup>35</sup>J. Wang and T. Y. Zhang, *Appl. Phys. Lett.* **86**, 192905 (2005).
- <sup>36</sup>J. Wang and T.-Y. Zhang, *Phys. Rev. B* **77**, 014104 (2008).
- <sup>37</sup>N. A. Pertsev, A. G. Zembilgotov, and A. K. Tagantsev, *Phys. Rev. Lett.* **80**, 1988 (1998).
- <sup>38</sup>W. J. Merz, *Phys. Rev.* **75**, 687 (1949).
- <sup>39</sup>W. P. Mason and B. T. Matthias, *Phys. Rev.* **74**, 1622 (1948).
- <sup>40</sup>J. Paul, T. Nishimatsu, Y. Kawazoe, and U. V. Waghmare, *Phys. Rev. B* **80**, 024107 (2009).
- <sup>41</sup>S. Wada, S. Suzuki, T. Noma, T. Suzuki, M. Osada, M. Kakihana, S. E. Park, L. E. Cross, and T. R. Shrout, *Jpn. J. Appl. Phys., Part 1* **38**, 5505 (1999).
- <sup>42</sup>S. E. Park, S. Wada, L. E. Cross, and T. R. Shrout, *J. Appl. Phys.* **86**, 2746 (1999).
- <sup>43</sup>Y. Okuno and Y. Sakashita, *Jpn. J. Appl. Phys.* **48**, 021403 (2009).
- <sup>44</sup>M. Iwata, Z. Kutnjak, Y. Ishibashi, and R. Blinc, *J. Phys. Soc. Jpn.* **77**, 065003 (2008).
- <sup>45</sup>O. E. Fesenko and V. S. Popov, *Ferroelectrics* **37**, 729 (1981).
- <sup>46</sup>S. Wada and T. Tsurumi, *Br. Ceram. Trans.* **103**, 93 (2004).
- <sup>47</sup>S. Wada, K. Yako, T. Muraishi, K. Yokoh, S. M. Nam, H. Kakemoto, and T. Tsurumi, *Ferroelectrics* **340**, 17 (2006).
- <sup>48</sup>S. Wada, K. Yako, K. Yokoo, H. Kakemoto, and T. Tsurumi, *Ferroelectrics* **334**, 17 (2006).
- <sup>49</sup>J. F. Nye, *Physical Properties of Crystals* (Oxford University Press, London, 1964).